Acta Cryst. (1979). A35, 564–569

$(4H)_2$–$4C$ Type Superstructure of $TiS_{1.46}$ as Determined by High-Resolution Electron Microscopy

BY Y. BANDO, M. SAEKI, Y. SEKIKAWA, Y. MATSUI, S. HORIUCHI

National Institute for Researches in Inorganic Materials, Sakura-mura, Niihari-gun, Ibaraki, Japan 300-31

AND M. NAKAHIRA

Okayama College of Science, Laboratory for Solid State Chemistry, Ridai-cho, Okayama, Japan 700

(*Received* 28 *September* 1978; *accepted* 6 *February* 1979)

Abstract

The superstructure of titanium sesquisulfide, $TiS_{1.46}$, is derived on the basis of 1 MV and 100 kV high-resolution electron microscope images. The crystal has monoclinic symmetry (pseudo-hexagonal) with lattice parameters $a = 5{\cdot}92$, $b = 10{\cdot}3$, $c = 22{\cdot}8$ Å and $\beta = 90°$. The space group is Cc. The metal vacancies are confined to every second metal layer and ordered within the layer. They are arranged in a stacking sequence of the $4C$-type along the c axis. The sulfur atoms are in the $4H$-type stacking sequence along the c axis.

Introduction

The titanium–sulfur system has a variety of structures in the range between TiS and TiS_2 (Jeannin, 1962). The structures are built up of various arrangements of metal vacancies as well as different stacking sequences of sulfur atom layers. Among them, the structure of nonstoichiometric $Ti_{1+x}S_2$ ($0{\cdot}1 < x < 0{\cdot}5$) was first determined by Wadsley (1957) and later refined by Norrby & Franzen (1970). The crystal is hexagonal with lattice parameters $a = 3{\cdot}42$ and $c = 11{\cdot}4$ Å. The space group is $P6_3mc$. The sulfur atoms are arrayed in hexagonal and cubic close-packing structures, which are alternately stacked along the c axis. This stacking sequence is refered to as $4H$-type. The titanium atoms are placed in the octahedral holes between sulfur atoms and these sites in every second cation layer are partly occupied. Norrby & Franzen (1970) assumed that the vacancies in the partly-filled metal layers were distributed in a random fashion. Moret, Huber & Comes (1976) have observed a diffuse scattering from $Ti_{1+x}S_2$ ($0{\cdot}17 < x < 0{\cdot}35$) with electron and X-ray diffraction and considered it to be due to short-range ordering of titanium atoms in the partly-filled metal layers. However, no superstructures which are formed due to an interlayer ordering have been reported in this system.

It has been shown that high-resolution electron microscopy is a very powerful means to study the arrangements of metal vacancies. Pierce & Buseck (1974) and Nakazawa, Morimoto & Watanabe (1975) have examined the superstructure in $Fe_{1-x}S$ and Horiuchi, Kawada, Nakano-Onoda, Kato, Matsui, Nagata & Nakahira (1976) in $V_{1-x}S$ with a 100 kV electron microscope. Horiuchi *et al.* (1976) have pointed out, on the basis of dynamical calculations, that the images appearing in the region between the first and second equal-thickness contours may be interpretable intuitively; the sites of metal vacancies were imaged as white spots. With an increase in the accelerating voltage, images more closely related to the object than those for 100 kV can be obtained, because many more scattered waves contribute to imaging. The 1 MV electron microscope constructed in our institute (Hitachi-1250 kV) can resolve to near 2·0 Å with axial illumination and a goniometer stage (Horiuchi, Matsui & Bando, 1976). It is expected that the sulfur atoms may be imaged directly with such a high resolving power.

In this paper, the superstructure of a $TiS_{1.46}$ crystal is determined from the 1 MV and 100 kV high-resolution electron microscope images. It is shown that the arrangement of sulfur atoms is detectable in the 1 MV structure image on the basis of the calculated image contrast.

Experimental procedure

Titanium sponge and sulfur powder were mixed with a composition of $TiS_{1.50}$. The purity of the starting materials was 99·0% for the titanium and 99·9% for the sulfur. They were first heated at 573 K for 24 h in an evacuated quartz tube. The product was ground and calcined at 1173 K for one week; the temperature was

0567-7394/79/040564-06$01.00

then lowered to 973 K and kept there for one week. The product was then cooled in air. The chemical composition of the final product was determined by oxidizing the sulfide to TiO_2 at 1073 K for 24 h. From the weight change during oxidation, the composition was estimated to be $TiS_{1\cdot46\pm0\cdot04}$.

The polycrystals obtained as above were crushed in an agate mortar to fragments of several microns. They were set on a holey carbon film and observed with the 1 MV and 100 kV (Hitachi-500 type) electron microscopes. The astigmatism of the objective lens was corrected by observing the granular image of the carbon film. The images obtained at underfocus values between 500 and 1000 Å for the 1 MV and at about 1000 Å for the 100 kV were interpretable intuitively. The direct magnification was $2\cdot5 \times 10^5$ times.

Results and interpretation

Electron diffraction patterns from the $TiS_{1\cdot46}$ crystals are shown in Fig. 1. Some reflections are indexed based on the NiAs subcell, although the subcell is not of NiAs type exactly in the present crystal. Remaining spots in Fig. 1 (*a*) and (*b*), which are taken with the incident electron beam parallel to the [001] and [$\bar{1}$10] directions of the subcell, respectively, exhibit the presence of a superstructure. They are situated at $h = m/3$, $k = n/3$ and $l = r/4$, where m, n and r are integers. No extra spots are observed in the diffraction pattern (*c*), taken with the incident electron beam parallel to the [010] direction of the subcell. The relations of the lattice parameters between the supercell and the NiAs subcell are $a = 2A_1 + A_2$, $b = 3A_2$ and $c = 4C$, where a, b and c are the lattice parameters for the supercell and A_1, A_2 and C for the NiAs subcell. The symmetry of the superstructure is apparently orthorhombic with lattice parameters $a = 5\cdot92$, $b = 10\cdot3$, $c = 22\cdot8$ Å and $\beta = 90°$. According to the extinction rule, however, it is truly monoclinic. The systematic absences were $h + k = 2n + 1$ for hkl and $l = 2n + 1$ for $h0l$. The possible space groups are therefore Cc (non-centrosymmetric) or $C2/c$ (centrosymmetric).

Fig. 2 shows a structure image obtained by the 1 MV electron microscope. The incident electron beam was parallel to the [010] direction of the subcell. The corresponding diffraction pattern is shown in Fig. 1(*c*), in which the position of the objective aperture is outlined. First and second equal-thickness contours are shown by arrows. Zigzag chains along the *c* axis are seen in the thinnest region outside the first contour. The zigzags repeat with a periodicity of about 11 Å along the *c* axis. In the region between the first and second contours, on the other hand, white spots are separately resolved. The separations of two adjoining white spots in the directions normal and parallel to the *c* axis are about 3 Å.

In order to interpret the observed image exactly, the intensity of each reflection was calculated dynamically for a structure model, which will be described later, using the multi-slice method derived by Cowley & Moodie (1957). The procedure for the calculation was the same as reported previously (Horiuchi *et al.*, 1976). The thickness of a slice was 3·4 Å and the interaction of 163 waves was taken into account. The image

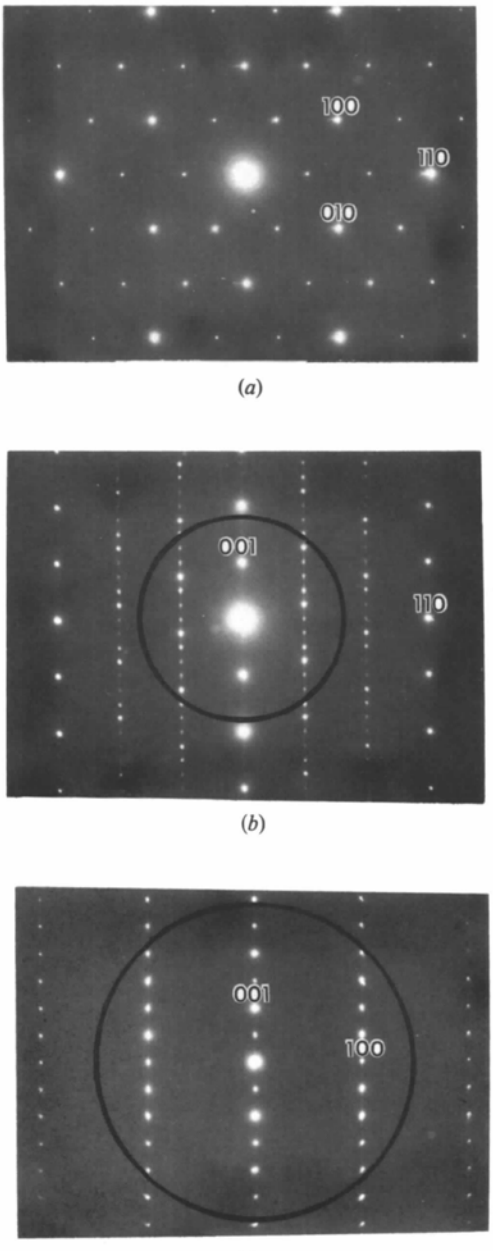

Fig. 1. Electron diffraction patterns from $TiS_{1\cdot46}$ crystal fragments. The incident electron beam is parallel to the (*a*) [001], (*b*) [$\bar{1}$10] and (*c*) [010] directions of the subcell. The indexed spots are fundamental reflections of a NiAs subcell.

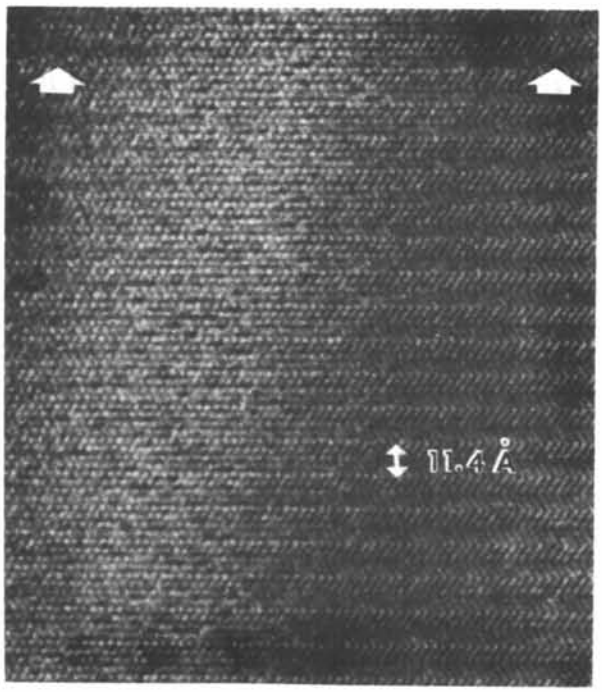

Fig. 2. A structure image obtained by a 1 MV high-resolution electron microscope. The electron beam is incident parallel to the [010] direction of the subcell. The corresponding diffraction pattern is shown in Fig. 1(*c*), in which the size of the objective aperture is outlined. First and second equal-thickness contours are shown by arrows.

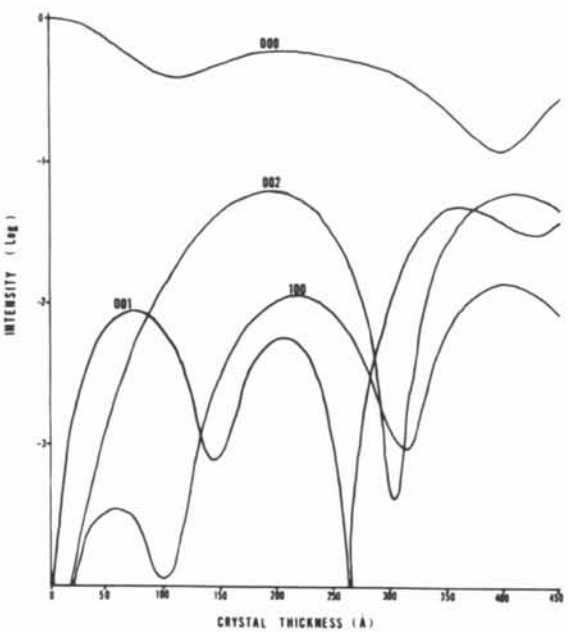

Fig. 3. Intensity of some scattered waves *versus* crystal thickness, calculated for the $(4H)_2$–$4C$ type superstructure of $TiS_{1\cdot46}$. The intensity of the incident electron beam is taken as unity.

contrast was then computed using the experimental values; the accelerating voltage was 1 MV, the spherical aberration coefficient was 10 mm and the aperture size corresponded to about 0·5 $Å^{-1}$ in reciprocal space. 23 waves were used for imaging.

Fig. 3 shows the calculated intensity *versus* crystal thickness curve. It is seen that the first contour appears at the thickness of about 110 Å and the second at about 400 Å. The simulated images are shown in Fig. 4(*b*) and (*c*), which are for the thicknesses of 20 and 143 Å, respectively. The simulated image in Fig. 4(*b*) approximately represents the projected potential of the crystal in Fig. 4(*a*); the zigzag chain with dark contrast is composed of titanium and sulfur atoms along the *c* axis. In other words, not only the titanium atoms but also the sulfur atoms contribute to the imaging. Since the separation between the neighboring sulfur and titanium atoms is as short as about 1·4 Å, each site is not resolved separately as a dark dot. The enlarged real image of the thin crystal region in Fig. 5(*a*) fits well the simulated image. This means that the structure model in Fig. 4(*a*) is valid, *i.e.* the sulfur atoms are arranged in a stacking sequence such as $..S_1S_2S_1S_3S_1..$ along the *c* axis, corresponding to the $4H$ type.

It is also interesting to interpret the image contrast of the thick region. The simulated image in Fig. 4(*c*) is in

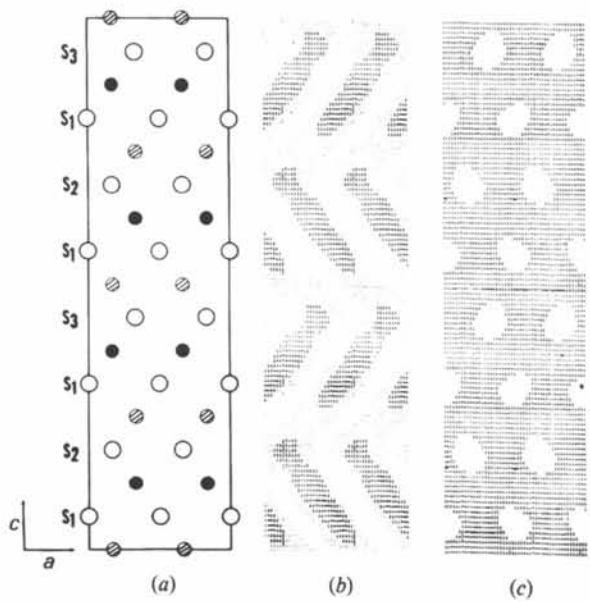

Fig. 4. Computer simulation images for the $(4H)_2$–$4C$ type superstructure of $TiS_{1\cdot46}$. (*a*) Superstructure model projected onto the (010) plane of the supercell. Open circles indicate sulfur atoms, dotted ones titanium atoms in the fully occupied metal layer and hatched ones titanium atoms in the partly occupied metal layer. Sulfur atoms are arranged in the $4H$-type of stacking sequence like $..S_1S_2S_1S_3S_1..$ along the *c* axis. (*b*) and (*c*) Computer simulation images, calculated for crystal thickness of 20 and 143 Å, respectively, at underfocus of 1100 Å.

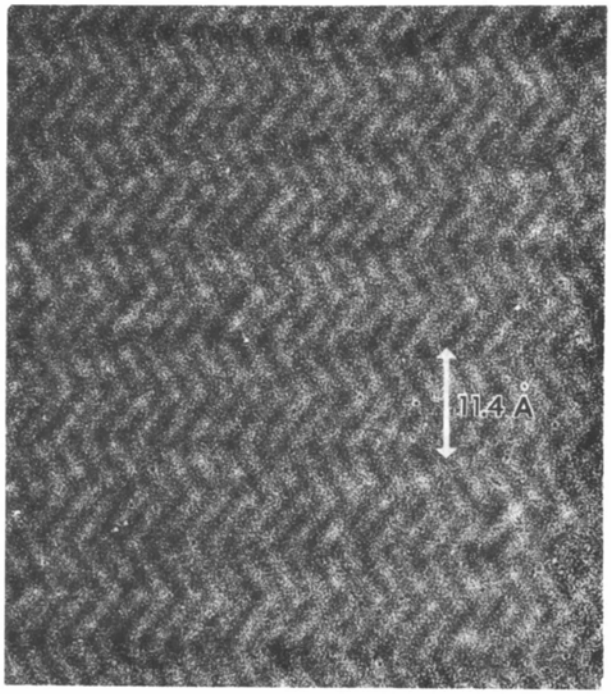

(*a*)

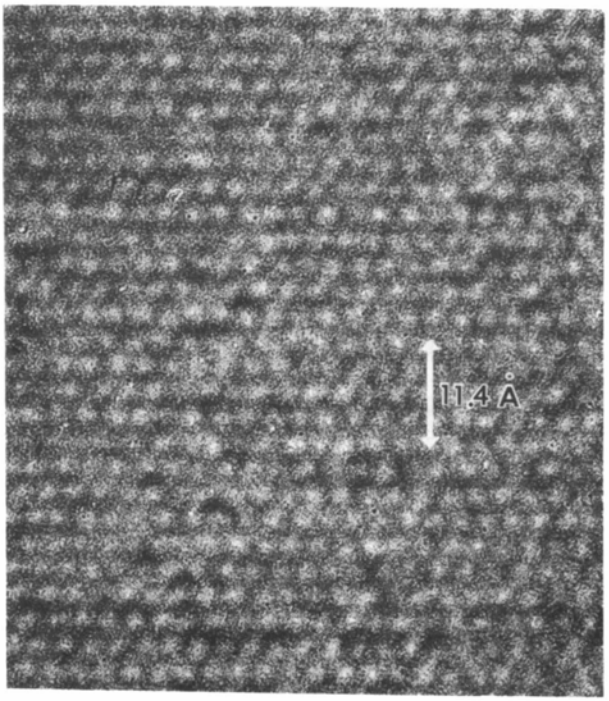

(*b*)

Fig. 5. High-magnification structure image of Fig. 2. (*a*) The image from the thinnest region outside the first contour. (*b*) The image from the thicker region between the first and second contours.

good agreement with the enlarged real image in Fig. 5(*b*). The image contrast of the thick crystal is quite different from that of the thin region in that only the white spots corresponding to the sites of sulfur atoms appear. It is generally known that the image contrast from the thick crystal is not interpretable intuitively. It might be accidental that each sulfur atom site is imaged in the present case. This however seems to confirm their stacking array, discussed above.

Fig. 6 shows a structure image of a very thin part of the crystal by the 100 kV electron microscope. The incident electron beam was parallel to the [$\bar{1}$10] direction of the subcell. The corresponding diffraction pattern is shown in Fig. 1(*b*), in which the size of the aperture is outlined. The aperture size corresponded to about 0·3 Å^{-1} in reciprocal space. From the previous calculation (Horiuchi *et al.*, 1976), we know that metal-vacancy-rich sites are imaged as white spots at the very thin part of the crystal as well as at the thicker part. A possible structure model read from the real image is shown in the figure. The separation of two adjoining white spots normal and parallel to the *c* axis are 5·9 and 5·7 Å, respectively. It is noticed that two neighboring metal-vacancy sites are imaged as a single white spot. The analysis of the next section makes it

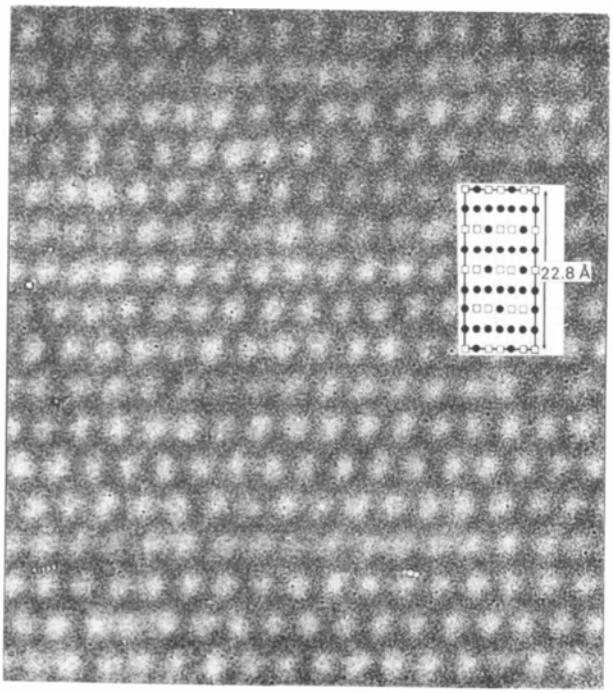

Fig. 6. A structure image obtained by a 100 kV electron microscope. The incident electron beam is parallel to the [$\bar{1}$10] direction of the subcell. The corresponding diffraction pattern is shown in Fig. 1(*b*), in which the position of the objective aperture is outlined. The structure model is inserted into the figure, in which open squares indicate the sites of metal vacancies and dark circles those of titanium atoms. The unit cell is outlined.

clear that the metal vacancies are regularly arranged in a superstructure with a dimension of 22·8 Å along the *c* axis, forming the stacking sequence of 4*C* type.

Description of the superstructure

The result of the electron diffraction patterns suggests that the space group of the superstructure is either *Cc* or *C*2/*c*. Since the sublattice of sulfur atoms has a non-centrosymmetric symmetry, the space group of the superstructure must be *Cc*.

Vacancies are confined to every second metal layer. The present composition requires that two thirds of the metal sites in such a layer are almost vacant. Circles *A*, *C* and *E* in Fig. 7(*a*) represent a set of possible sites of cations within the layer. When the sites *A* are occupied, the sites *C* and *E* must be kept vacant within the layer. Circles *B*, *D* and *F* heavily drawn are another possible set of cation sites. The superstructure is built up as in Fig. 7(*b*), in which is shown the projection in the *a* direction. We first assume that the sites *A* are occupied in layer 1. In layer 3, the sites *C* must be occupied because of the symmetry element of the glide *c*. It is then found from the analysis of the array of the white spots in Fig. 6 that the sites *B* are occupied by layer 2. Layer 4 has the cation arrangement of *D* due to the symmetry operation. It is clear that Fig. 6 represents the projection not of the [100] but of the [$\bar{1}$10] direction of the supercell.

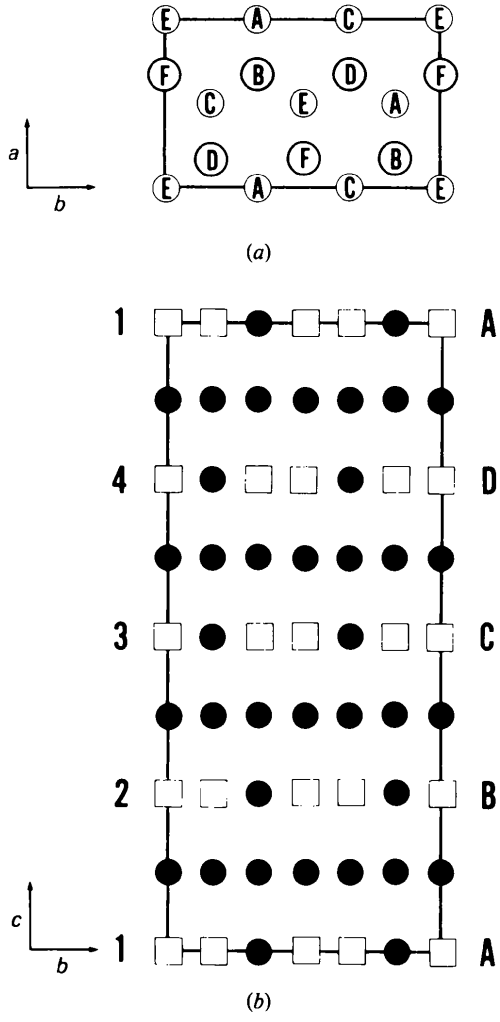

Fig. 7. The $(4H)_2$–4*C* type superstructure of $TiS_{1.46}$. (*a*) A set of possible sites of cations within the partly-filled metal layer. Light circles *A*, *C* and *E*, and heavy ones *B*, *D* and *F* mean sites within the same respective layer. (*b*) Superstructure projected onto the (100) plane. Open squares show the sites of metal vacancies and dark circles those of titanium atoms. The sulfur atoms are not shown for simplicity. The unit cell is outlined.

The stacking sequence of the metal layers can then be represented as $..V_AGV_BGV_CGV_DGV_A..$ along the *c* axis, where V_A, V_B, V_C and V_D mean the defective layers and *G* the completely filled layers. The stacking periodicity is 4*C* along the *c* axis, where *C* is the lattice parameter of the NiAs subcell.

The layers of sulfur atoms are interleaved with the complete and defective metal layers and form a stacking sequence of the 4*H* type, as mentioned above relating to Figs. 2 to 4. The superstructure consists of eight sulfur layers and eight metal layers, and is represented as $..V_AS_1GS_2V_BS_1GS_3V_CS_1GS_2V_DS_1GS_3V_A..$ along the *c* axis; sulfur atoms are, however, abbreviated in Fig. 7. It seems reasonable, therefore, to describe the superstructure as a $(4H)_2$–4*C* type, *i.e.* the combined representation of the arrangements of sulfur atoms and metal vacancies.

Jellinek (1957) has found two types of superstructures for crystals with composition near Cr_2S_3. $Cr_{0.69}S$ has a 2*C*-type superstructure, while $Cr_{0.67}S$ a 3*C* type. The slight difference in chemical composition resulted in a different superstructure. One may therefore expect to observe different superstructures in the present titanium–sulfur system too. In fact, we have recently found a $(4H)_3$–6*C* type superstructure for the composition $TiS_{1.50}$. The result of the structure analysis will be reported elsewhere.

The authors would like to express their deep gratitude to Drs M. Nakano-Onoda, H. Nakazawa and I. Kawada for valuable discussions.

References

Cowley, J. M. & Moodie, A. F. (1957). *Acta Cryst.* **10**, 609–619.

Horiuchi, S., Kawada, I., Nakano-Onoda, M., Kato, K., Matsui, Y., Nagata, F. & Nakahira, M. (1976). *Acta Cryst.* A**32**, 558–565.

HORIUCHI, S., MATSUI, Y. & BANDO, Y. (1976). *Jpn. J. Appl. Phys.* **15**, 2483–2484.
JEANNIN, Y. (1962) *Ann. Chim. (Paris)*, **7**, 57.
JELLINEK, F. (1957). *Acta Cryst.* **10**, 620–628.
MORET, R., HUBER, M. & CÒMES, R. (1976). *Phys. Status Solidi, A*, **28**, 695–700.
NAKAZAWA, H., MORIMOTO, N. & WATANABE, E. (1975). *Am. Mineral.* **60**, 359–366.
NORRBY, L. J. & FRANZEN, H. F. (1970). *J. Solid State Chem.* **2**, 36–41.
PIERCE, L. & BUSECK, P. R. (1974). *Science*, **186**, 1209.
WADSLEY, A. D. (1957). *Acta Cryst.* **10**, 715–716.

Acta Cryst. (1979). A**35**, 569–571

The Crystal Structure of Deuteroammonia between 2 and 180 K by Neutron Powder Profile Refinement

BY A. W. HEWAT AND C. RIEKEL

Institut Max von Laue–Paul Langevin, BP 156X, Grenoble, France

(*Received* 28 *December* 1978; *accepted* 9 *February* 1979)

Abstract

The structure of ND_3 has been refined by neutron powder profile analysis at 2, 77 and 180 K to a resolution of sin $\theta/\lambda = 0{\cdot}85$ Å^{-1}. No orientational phase transition was found in this range. However, even at 2 K, a strong librational motion exists. The N–D bond length, after correction for libration, is constant with temperature (1·06 Å), as are the D–N–D angles (107·5 ± 0·2°). This bond length is 5% longer than that found in the free molecule, because of hydrogen bonding, but the bond angles are virtually identical.

Introduction

Solid ammonia has one of the simplest molecular structures. The molecules are bound together by rather weak hydrogen bonds involving the lone pair of electrons, which with the three H atoms make up an almost regular rigid tetrahedron around the N atom (Olovsson & Templeton, 1959; Reed & Harris, 1961).

NH_3 in its solid state is an ideal material for the study of the dynamics of simple molecular crystals. Righini & Klein (1978) have set up a lattice-dynamical model, which has been used by Dolling, Powell & Pawley (1978) to explain their inelastic neutron scattering results. Such model calculations require a precise knowledge of the structure, and this was one justification for the present study.

The structure of NH_3 and ND_3

Olovsson & Templeton (1959) studied single crystals of NH_3 and ND_3 by photographic X-ray techniques at 77 and 113 K. A neutron powder diffraction study of ND_3 was made by Reed & Harris (1961) at 77 K. Both studies were limited by rather low resolution, *i.e.* sin $\theta/\lambda = 0{\cdot}58$ Å^{-1} (Olovsson & Templeton) and 0·46 Å^{-1} (Reed & Harris). However, both agreed on the space group $P2_13$ (T^4) in which the atoms are placed as follows: 4 N at u,u,u with $u \simeq 0{\cdot}21$; 12 H at x,y,z with $x \simeq 0{\cdot}37$, $y \simeq 0{\cdot}26$, $z \simeq 0{\cdot}11$. The refined coordinates (Table 1) agree within the rather large experimental errors.

Experiment

The experiment was performed in two parts, both on the D1A high-resolution powder diffractometer (Hewat & Bailey, 1976) using a He gas flow cryostat. For the first part, data were collected at 77 K with a wavelength of 1·5 Å up to sin $\theta/\lambda = 0{\cdot}66$ Å^{-1}. Later, more precise results were collected at 2 and 180 K with a wavelength of 1·17 Å to extend the resolution to sin $\theta/\lambda = 0{\cdot}85$ Å^{-1}.

ND_3 (Saclay, 99% deuterated) was purified over Na and distilled. Some difficulties were experienced in preparing the powder sample. In the first attempt, ND_3 was sublimed from a solid-CO_2-cooled reservoir into a liquid-N_2-cooled vacuum-tight vanadium can. However, even at 77 K the intensities of some lines in the neutron diffraction pattern changed within a few hours, indicating the growth of crystallites in the sample. A similar effect was found when liquid ND_3 was snap frozen to 77 K. Finally, liquid ND_3 was frozen into a mortar immersed in a bath of liquid N_2 in a dry glove bag. It was then relatively easy to crush the solid ND_3 into a fine powder and to fill the vanadium can which was also cooled to liquid N_2 temperature. The can with about 6 g of ND_3 was transferred to the cryostat while still cold, and the temperature raised briefly to boil off any remaining N_2. Careful checks for preferred orientation during the experiments revealed

0567-7394/79/040569-03$01.00